International Journal of Medical, Medicine and Health Sciences
ISSN: 2517-9969
Vol:7, No:8, 2013

Segmenting Ultrasound B-Mode Images Using RiIG Distributions and Stochastic Optimization

N. Mpofu and M. Sears

***Abstract*—**In this paper, we propose a novel algorithm for delineating the endocardial wall from a human heart ultrasound scan. We assume that the gray levels in the ultrasound images are independent and identically distributed random variables with different Rician Inverse Gaussian (RiIG) distributions. Both synthetic and real clinical data will be used for testing the algorithm. Algorithm performance will be evaluated using the expert radiologist evaluation of a soft copy of an ultrasound scan during the scanning process and secondly, doctor's conclusion after going through a printed copy of the same scan. Successful implementation of this algorithm should make it possible to differentiate normal from abnormal soft tissue and help disease identification, what stage the disease is in and how best to treat the patient. We hope that an automated system that uses this algorithm will be useful in public hospitals especially in Third World countries where problems such as shortage of skilled radiologists and shortage of ultrasound machines are common. These public hospitals are usually the first and last stop for most patients in these countries.

***Keywords*—**Endorcardial Wall, Rician Inverse Distributions, Segmentation, Ultrasound Images.

I. Introduction

THE on-going improvements in the design of medical imaging modalities like X-Rays, Ultrasounds (US) and Computerized Tomography (CT) have revolutionized medical diagnosis. These technologies are used to image internal human organs and they provide extremely good views of these internal anatomies [1]. The use of these tools allows improved diagnosis, surgical planning, radiotherapy and tracking of disease progress.

Medical image analysis is aimed at processing, measuring, and quantifying embedded structures in medical images with improved accuracy, repeatability and efficiency. However, the study of medical images is heavily dependent on the radiologists' visual interpretation. This process is not only subjective and time consuming, but also depends on the experience of the radiologist [2]. Furthermore, the size, shape and appearance of anatomical structures can vary between individuals depending on a variety of factors including age and gender [3].

While it is true that modern imaging techniques present very good views of human internal anatomy, there is still limited use of computers for an automated quantification and analysis of the large amounts of medical data provided by these imaging modalities[2]. This limitation makes automated medical image analysis an important research field. The use of computer-aided systems also helps alleviate some of the challenges faced by the radiologist [2].

Deformable models are among the algorithms that have been developed to aid doctors [2]. These algorithms search an image for a particular human organ and attempt to delineate the exact boundary of the anatomical structure. The size, shape, location and appearance of the extracted boundary serve as useful tools in helping doctors reach the best conclusions concerning the patient's health [2].

US medical image segmentation has been an active research area for many years. Difficulties with US medical image segmentation include their low SNR, attenuation, diffraction and the presence of speckle. Generally, US images have a grainy appearance, which is the result of a spatial stochastic process known as speckle. Speckle also causes low contrast of boundaries

Currently, one of the most frequently used US imaging techniques for diagnostic purposes is the Brightness mode (B-mode). Speckle in US B-mode scans constitutes an issue that is not yet completely understood. An open question is: Should the speckle in the image of the functional tissue of an organ (as opposed to the supporting and connecting tissue) be seen as image signal or should it be seen as undesirable noise [4]? Using stochastic analysis, many researchers of US B-mode scanning have described the character of the US speckle as random noise. These researchers have obtained evidence of this by comparing their predictions to measurements of image speckle. Examples include work done in [4]-[7].

Conversely, there are researchers who view speckle in some clinical US B-scan images as associated with the microstructure of tissue parenchyma. Such a view qualifies speckle to be considered as image signal and thus can be used as an aid for diagnosis. These include the work described in [8]-[10]. Researchers who view speckle as noise in US images first clear the speckle before doing any segmentation on the image. Because of the latter viewpoint, we propose to directly segment our images without first smoothing out speckle.

For segmenting the image, we use a deformable model. Since speckle appears random, it can cause false positives in a deformable model algorithm that directly searches an US image for the edges of a particular anatomical structure. As a result, the evolving model often ends up trapped in locations that are far from the true boundary. The main idea of our research is to use the RilG distribution [11] in a Bayesian framework to assist the deformable model segment US images. The approach uses an optimization procedure that we propose to solve using the exploration/selection algorithm proposed in [12] together with the steepest ascent algorithm.

N. Mpofu is with the University of Witwatersrand, Johannesburg, 2000, South Africa (phone: 0027-11-7176195; fax: 0027-11-717-6199; e-mail Nontokozo.Mpofu@wits.ac.za).

M.Sears is with the University of Witwatersrand, Johannesburg, 2000, South Africa (phone: 0027-11-7176183; fax: 0027-11-717-6199; email: Michael.Sears@wits.ac.za).

The Bayesian approach relies on the work developed in [13], [14].

This paper is organized as follows. In the next section we give a brief overview of the how US interacts with body tissue. We follow this section by giving a brief overview of active shape models. We then provide a theoretical framework of the Bayesian estimation of the segmentation problem, which results in us formulating a cost problem. We propose solving this cost problem using a combination of the estimation/selection algorithm together with the steepest ascent algorithm. Before we conclude, we show one of the steps we do in fitting the RilG distribution to our data set.

II. Interactions with Tissue

A. Modes of Interaction

The transducer (a component of an US probe) consists of one or more piezoelectric elements. These piezoelectric elements are able to generate an US wave when they are excited by an electrical wave. As the wave moves through the body and encounters various tissues, some of it is reflected back to the transducer whereas the rest of it is transmitted further into the body. The reflected energy, when it reaches the transducer, is transmitted back to electrical energy for further processing before producing the image displayed on the US screen [15]. The time frame it takes for the echo to return gives an idea of where exactly the material is [26]. The medium that the sound wave travels through impacts its speed. For most body tissue, the sound speed lies in the 1,500m/s, for example, in fat, the speed is 1,450m/s, in kidney, it is 1,565m/s and in amniotic fluid, the speed is 1,540m/s [16].

As the sound wave interacts with the body tissues, it loses its energy. This is called attenuation. Four different ways that the sound interacts with tissue have been identified. These are incident reflection, off-angle reflection, specular reflection and scatter. Scatter reflection plays an important role in US image formation as it helps us identify a certain body organ type, for example, whether it is a liver or a kidney [16].

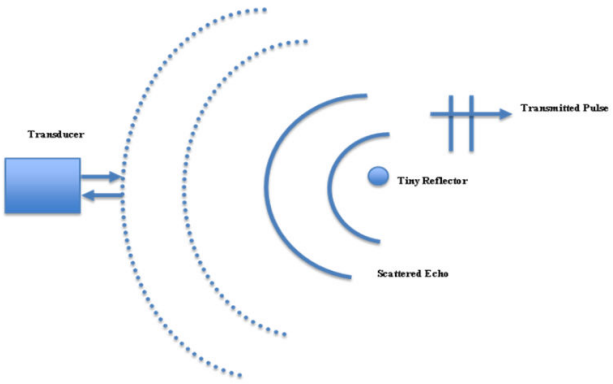

Fig. 1 Scatter Example

Fig 1 above, adapted from [16], shows an example of scatter whereby the solid curves represent the sound waves scattered into numerous directions when the transmitted signal encounters a tiny reflector along its path. The dotted curves mean that the scattered sound waves over time are reflected back to the transducer.

If the scattering medium is modeled as a distribution of independent and identically distributed random variables, then the detected signal from a given resolution cell can be as:

$$E = X + jY = Ae^{j\varphi} = \sum_{i=1}^{N} a_i e^{j\phi} \quad (1)$$

Where N is the number of scatteres in the cell, a_i is the amplitude, ϕ_i is the phase of the scatterer, X and Y are the in-phase (I) and the quadrature (Q) components respectively [11]. Researchers have modeled the amplitude statistics of coherent images for some timenow. Some of the current existing algorithms utilize a Bayesian approach where accurate locale statistical models for the speckled and speckle free images become essential. Furthermore, it becomes a goal for the users of B-mode US images to accurately classify and characterize image regions [11]. Distributions for the local brightness of the speckle pattern of US B-mode scan images have been proposed in the literature. These include the Rayleigh distributions, generalized Rician distribution, the K-distribution, the Nakagami distributions and recently, the RilG distributions [22]-[25], [11].

III. Active Shape Models (ASM)

An ASM is a technique that is used to build compact models of a shape and appearance of almost any flexible object. An ASM can also be used to search an image for a new shape example. In an ASM, objects are represented as labeled points and the statistics of their co-ordinates are examined over a number of training models, for example, the Point Distribution Models (PDMs) [17].

A. Training Set

The features of interest in medical images are represented by sets of labeled points. This method works by modeling, as the shape varies, how different labeled points (landmarks) tend to move together [18]. The following criteria can be used in the selection of landmark points: easily located biological marks, points of high curvature and the 'T' junctions between boundaries [19]. These points are hardly enough for a shape representation. Therefore, the additional points that can be added are those that lies on boundaries. These points will have to be placed equally within well-defined landmarks [19].

B. Aligning a Set of Training Shapes

For the purpose of comparing equivalent points from different shapes, the coordinate points of these shapes are aligned in the same way with respect to a set of axes. The Generalized Procrustes Analysis (GPA) is used for aligning these shapes [20]. Fig 2 shows an example of shape alignment. The code used was adapted from [27].

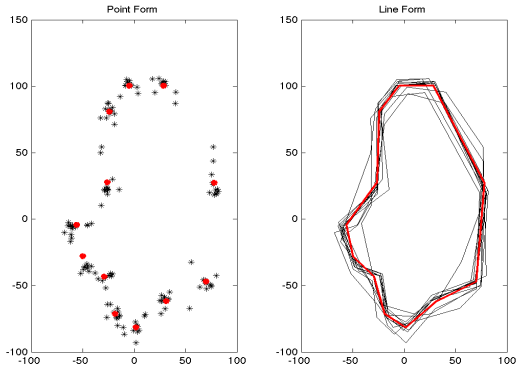

Fig. 2 Shape alignment examples for shapes like Fig 3

Fig. 3 Shape example

C. Capturing the Statistics of a Set of Aligned Shapes

Let each shape be represented by a total of *n* points. A single point in a 2*n* dimensional space can be used to represent each example of the aligned shape. In this 2*n* dimensional space, a set of *N* example shapes produces a cloud of *N* points. An assumption can then be made that these points lie within an 'Allowable Shape Domain' [18], (a space region), and that an indication of the shape and the size of this region can be obtained using these points.

Each one of the 2*n* dimensional points within this domain includes a set of landmarks. These landmarks have a shape that is in a strong sense, similar to those in the training set. New shapes can then be generated by just moving about the domain in a systematic way [18].

If x_i is a vector that describes the *n* points of the i^{th} shape in the set:

$$x_i = (x_{i0}, y_{i0}, ...x_{ik}, y_{ik}, ..., x_{in-1}, y_{in-1})^T \quad (2)$$

where (x_{ij}, y_{ij}) is the j^{th} point of the i^{th} shape. The mean shape $\bar{x}$ is calculated as follows:

$$\bar{x} = \frac{1}{N}\sum_{i=1}^{N} x_i \quad (3)$$

The modes of variation, that is, the ways in which the points of the shape tend to move together, can be found by applying PCA to the deviations from the mean as follows:

$$dx_i = x_i - \bar{x} \quad (4)$$

The covariance matrix is then computed using the following equation:

$$S = \frac{1}{N}\sum_{i=1}^{N} dx_i dx_i^T \quad (5)$$

Let λ_k be the k^{th} eigenvalue of the k^{th} eigenvector p_k, where $k = 1,2,...2n$, and $\lambda_k \geq \lambda_{k+1}$, then the modes of variation of the points of the shape are described by p_k, and the unit eigenvectors of *S* are described such that:

$$S_{pk} = \lambda_k p_k \quad (6)$$

The most significant modes of the variation are described by the largest eigenvectors of the covariance matrix that corresponds to the largest eigenvalues. A small number $t << 2n$ explains almost the total variance [3]. The following equation is then used to calculate a new model:

$$x \approx \bar{x} + P\,\boldsymbol{b} \quad (7)$$

where $P = (p_1, p_2, ..., p_t)$ is the matrix of the first *t* eigenvectors and $\boldsymbol{b} = (b_1, b_2, ..., b_t)^T$, the weight vector of the *t* eigenvectors.

The criteria for determining the number of eigenvectors *t* to be used is chosen so that the eigenvectors will represent a certain amount of the variation in the training set, usually ranging from 90% to 95% so that new examples of the shape parameter can be generated by varying the parameters λ_k within a suitable limit [21]. Fig. 4 below shows an example of how the mean shape of example shapes shown in Fig 2, can vary within the "Allowable Shape Domain".

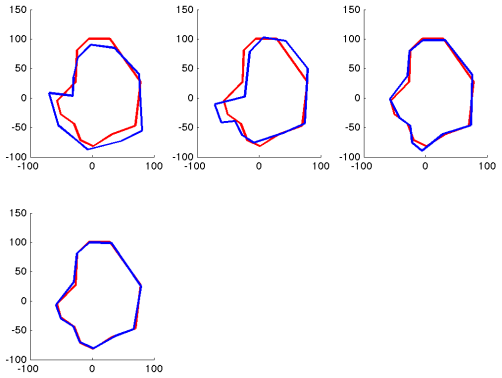

Fig. 4 An example of how the mean shape can vary

Fig 5 below shows an example of a set of *m* pixels taken below and above each landmark of an example image.

Fig. 5 An example of landmark profiles

D. Gray-level Appearance

The normalized derivative of the profiles sampled perpendicular to the landmark contour and centered at the landmark is the gray-level appearance model that describes the local texture feature around each landmark. A total number of *m* points are chosen on either side of the each landmark point. Estimation of the next best landmark position during the searching process is done using this gray level information. The symbol g_{ij} is used to denote the gray level profile of the j^{th} landmark in the i^{th} image. This represents a 2*n*+1 dimensional vector. Thus:

$$g_{ij} = \lfloor g_{ij0}, g_{ij1}, \ldots, g_{2n+1} \rfloor \quad (8)$$

where g_{ijm} is the gray level intensity of a corresponding pixel and $m = 0,1,\ldots,2n+1$. The derivative along the profile is estimated by:

$$dg_{ij} = \lfloor g_{ij1} - g_{ij0}, g_{ij2} - g_{ij1}, \ldots, g_{ij(2n+1)} - g_{ij(2n)} \rfloor \quad (9)$$

The derivative profile is then normalized by:

$$y_{ij} = \frac{dg_{ij}}{\sum_{k=0}^{2n} |dg_{ijm}|} \quad (10)$$

where $dg_{ijm} = g_{ij(m+1)} - g_{ijm}$. The covariance for the normalized derivative profile is given by

$$C_{yj} = \frac{1}{N}\sum_{i=1}^{N}(y_{ij} - \bar{y})(y_{ij} - \bar{y})^T \quad (11)$$

and $\bar{y}$ is the mean profile.

For the shape model to fit accurately to the object of interest in the image, the ASM utilizes the obtained information from the modeling of the gray level statistics around each landmark to determine the desired movement or adjustment of each landmark. However, the form of the fit measure is difficult to determine. If the shape model represents the target feature boundaries and strong edges of the object, then a useful measure is the distance between a given model point and the nearest strong edge in the image. Euclidean or Mahalanobis distance is often used in such cases [19]. The equation given below shows how the Mahalanobis distance can be used:

$$f(y) = (y - \bar{y}_j)^T C_{ij} (y - \bar{y}_j) \quad (12)$$

Therefore, minimizing is the same as maximizing the probability of *y* according to a given Gaussian distribution.

The current shape is then aligned with the new shape (the one determined by the new set of landmark points). This step produces the next best shape. The parameters are then adjusted and a new model is generated. The process of searching for a new shape, aligning the two shapes, adjusting the parameters and generating a new shape is repeated until convergence is reached [19].

However, ASMs tend to perform poorly on US images as US images have a low SNR, have low attenuation and contain speckle. Using the Bayesian framework, deformable models have been used in conjunction with speckle models to segment B-mode US images [13], [14].

IV. Bayesian Estimation of the Contour Position

In this paper, we propose modeling the gray level statistics of blood and tissue in US B-mode images of the human heart using the RilG distributions in conjunction with a deformable model. Our original deformable model is the mean of a set of endocardial wall images. This mean shape is computed using the ASM. The RilG model is a new statistical distribution that was recently introduced in [11]. This statistical distribution is specifically for non-Rayleigh amplitude statistics and has three parameter α (controls the distribution steepness), β (determines the distribution skewness) and ∂ (dispersion parameter). The presence of three parameters makes the distribution very flexible and thus the density function can take many forms. The RilG distribution is a mixture of the Rician distribution with the Inverse Gaussian Distribution. The RilG model for the intensity distribution is defined in [11] as:

$$p_R(r) = \sqrt{\frac{1}{2\pi}}\alpha^{\frac{3}{2}}\partial \exp(\partial\gamma)$$

$$* \frac{\sqrt{r}}{(\partial^2 + i)^{\frac{3}{4}}} k_{\frac{3}{2}}(\alpha^2 + i) I_0(\beta\sqrt{i}) \quad (13)$$

where $\gamma = \sqrt{\alpha^2 - \beta^2}$, $K_{\frac{3}{2}}(.)$ is the modified Besselfunction

of the second kind and order $\frac{3}{2}$, and $I_0(.)$ is the modified Bessel function of the first kind and zero order.

Following some of the ideas in [13], [14], we formulate the *a posterior* distribution using Bayes'rule as follows:

$$p(C,\alpha,\beta,\partial \mid I) = \frac{p(I \mid C,\alpha,\beta,\partial)\,p(C,\alpha,\beta,\partial)}{p(I)} \quad (14)$$

where*C* is an initial *a priori* contour whose *a priorI* probability is *p(C)* and is the mean contour computed from the ASM. The data likelihood is given by $p(I \mid C)$.

A. Data Likelihood

The data likelihood is given by *p(I|C)* and *p(I)* is a normalizing constant and *I* is the image. Since our data likelihood is based on the RilG model and there are two regions, *rb*(for blood) and *rt*(for tissue), the data likelihood then becomes:

$$p(I \mid C,\alpha,\beta,\partial) = \prod_{i\in rb} p(A_i \mid C,\alpha,\beta,\partial) * \prod_{j\in rb} p(A_j \mid C,\alpha,\beta,\partial) \quad (15)$$

which reduces to:

$$p(I \mid, par) = \prod_{i\in rb}\left[\sqrt{\frac{1}{2\pi}}\alpha_b^{\frac{3}{2}}(C)\partial_b(C)\exp(\partial_b(C)\gamma) * \frac{\sqrt{r}}{(\partial_b^2(C)+A_i)^{\frac{3}{4}}} k_{\frac{3}{2}}(\alpha_b^2(C)+A_i) I_0(\beta_b(C)\sqrt{A_i})\right] * \prod_{j\in rt}\left[\sqrt{\frac{1}{2\pi}}\alpha_t^{\frac{3}{2}}(C)\partial_t(C)\exp(\partial_t(C)\gamma) * \frac{\sqrt{r}}{(\partial_t^2(C)+A_j)^{\frac{3}{4}}} k_{\frac{3}{2}}(\alpha_t^2(C)+A_j) I_0(\beta_t(C)\sqrt{A_j})\right] \quad (16)$$

where A_i is the brightness value of the i^{th} sample, *par*are the parameters and $\alpha_b, \beta_b, \partial_b, \alpha_t, \beta_t, \partial_t$, are the parameters of the RilG density function, depending on the contour position as well as on the regions*rb*'s and*rt*'s brightness respectively.

B. Prior Energy Term

This term penalizes the deviation of the deformed template from the original prototype $\overline{C}$, (the mean of the shape obtained using the ASM). The deformed template (our new *C)* can then be generated using the following equation:

$$C = M(s(1+ds),(\theta+d\theta))(\overline{C}+\phi(b+db))+(t+dt) \quad (17)$$

where*b* is the shape parameter, ϕ are the eigenvectors, *s,* θ and *t* are the pose parameters. *M* is a matrix for a rotation followed by scaling and *t* is a translation vector. The shape and the pose parameters need to be determined. The adjustment *db* can be found using the equation

$$db = \phi^T(dS) \quad (18)$$

and*dS* is computed as:

$$dS = M(s^{-1}(1+ds)^{-1},-(\theta+d\theta))(Y-t-dt)-S_0 \quad (19)$$

and*Y* represents the next best set of points to move to.

B. Maximum a Posterior

The search for $\hat{\theta}_{MAP}$ is then given by the equation

$$\hat{\theta}_{MAP} = \prod_{i\in rb}\left[\sqrt{\frac{1}{2\pi}}\alpha_b^{\frac{3}{2}}(C)\partial_b(C)\exp(\partial_b(C)\gamma) * \frac{\sqrt{r}}{(\partial_b^2(C)+A_i)^{\frac{3}{4}}} k_{\frac{3}{2}}(\alpha_b^2(C)+A_i) I_0(\beta_b(C)\sqrt{A_i})\right] * \prod_{j\in rt}\left[\sqrt{\frac{1}{2\pi}}\alpha_t^{\frac{3}{2}}(C)\partial_t(C)\exp(\partial_t(C)\gamma) * \frac{\sqrt{r}}{(\partial_t^2(C)+A_j)^{\frac{3}{4}}} k_{\frac{3}{2}}(\alpha_t^2(C)+A_j) I_0(\beta_t(C)\sqrt{A_j})\right] * C = M(s(1+ds),(\theta+d\theta))(\overline{C}+\phi(b+db))+(t+dt) \quad (20)$$

Equation (20) can be numerically solved. We propose estimating the optimal values of the parameters using the exploration/selection algorithm in combination with gradient ascent, which is workthat is currently, still inprogress. We also note that there are possible variations within the tissue region.

V. Curve Fitting

We conducted an experiment on each of our images whereby we independently investigated the intensity distributions of the blood and tissue regions in our images. In this experiment, we selected regions of homogeneous brightness within the images, computed their histograms and compared these histograms with the RilG distribution. Figs. 6 and 7 below show an example of a sample image and a selected region of interest. Fig 8 is the histogram of the selected image portion.

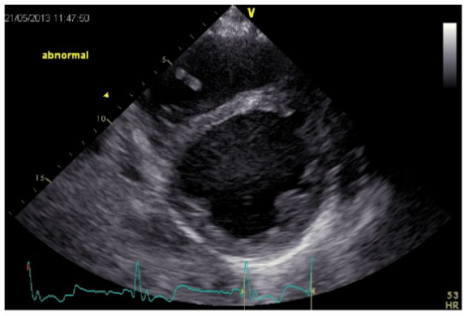

Fig. 6 An example image

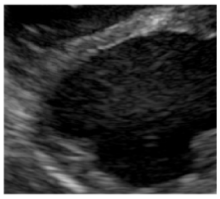

Fig. 7 Selected portion of the image in Fig 6

We also computed a chi-square test for each image. For the curve to fit the histogram, a number of iterations have to be made in search of the optimal parameters. The optimal parameters can be computed using either the iterative maximum likelihood method or the iterative moment method. Both methods were proposed in [11]. Fig. 9 shows our first attempt to fit the RilG model into the histogram in Fig 8. The Goodness of Fit test shown in Table I, proves that this is not the optimal curve as yet. In Table I, the initial parameter values for α, β and $\hat{\partial}$ are 9.8760e-09, 9.9328e-16 and 0.1228, respectively. A total of 2 degrees of freedom was used. The test-statistic value was 1.0137e+04 and the chi-square critical value: (significance level – 0.05) $\chi_{2,(0.05)}$ was 5.991 Curve Fitting was done using the modified code adapted from [28]. The format of Table I was adapted from [29].

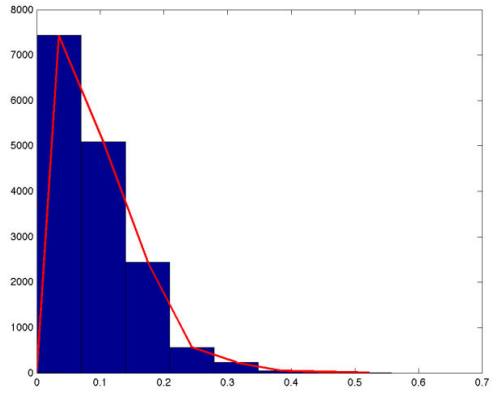

Fig. 8 Histogram for the selected image portion

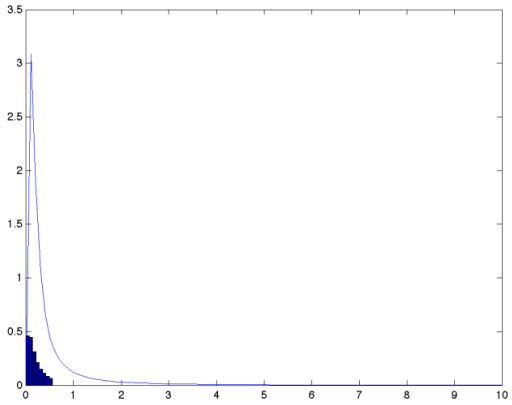

Fig. 9 First iteration

TABLE I
Intermediate Values for the RilGGOF T/Test

Row	InitEnd	CellProb	Expected 1.0e+03*	Observed	(e-o)^2/e 1.0e+03
1	0.0697	0.4621	7.3250	7433	7.3250
2	0.1394	0.4456	7.0625	5091	7.0625
3	0.2090	0.3141	4.9789	2442	4.9789
4	0.2787	0.2141	3.3936	565	3.3936
5	0.3484	0.1510	2.3941	231	2.3941
6	0.4181	0.1111	1.7603	54	1.7603
7	0.4878	0.0847	1.3420	25	1.3420
8	0.5575	0.0665	1.0543	10	1.0543
	Total	**1.8491**	**2.9311e+04**	**15851**	

VI. Conclusion

This paper proposed a novel algorithm for the segmentation of ultrasound B-mode scan images using the RilG model together with the steepest ascent algorithm. Using synthetic data, we have shown how the mean shape of a set of shapes can be derived using the ASM. Since the ASM performs badly on US images, we have discussed an alternative method that has been used in the literature for segmenting ultrasound. This method uses a model of the speckle statistics of an image in conjunction with a deformable model. We thus chose the RilG

model because of its flexibility and its capability to fit into various shapes. We then fit the model into our set of images which we followed by a theoretical description of our Bayesian estimation of the contour position in the image. This resulted in the formulation of a cost function which we propose to numerically solve using the estimation/selection algorithm together with the steepest algorithm theorem and this is the work that we are currently doing.

ACKNOWLEDGMENT

We would like to express our gratitude to the University of Wits Dean's Spark Fund and the Centre for Higher Performance and Computing (CHPC) for funding this research.

REFERENCES

[1] T. McInerney and D. Terzopoulos, "Deformable models in medical image analysis in mathematical methods," pp 171– 180. IEEE,1996.
[2] [H. C. Inyiama Engr. V. C. Chijindu and Engr. G.Uzedhe, "Medcal imagesegmentation methodologies: A classified overview,"*African Journal of Computing and ICT*, 2006.
[3] T.F. Cootes, A. Hill, C.J. Taylor, and J. Haslam."Use of active shape models for locating structures in medical images,"*Image and vision computing.*vol. 12, no. 6, pp..355–365, 1994.
[4] R.F. Wagner, S.W. Smith, J.M. Sandrik, and H. Lopez,. "Statistics of speckle in ultrasound b-scans,"*IEEE Trans. SonisUltrasonics*.,vol. 30, no. 3, pp. 156–163, 1983.
[5] P. Atkinson and MV Berry,. "Random noise in ultrasonic echoes diffracted by blood,"*Journal of Physics A: Mathematical, Nuclear and General,*vol.7, no. 11, pp. 1293, 2001.
[6] C.B. Burckhardt, "Speckle in ultrasound b-modescans. Sonics and Ultrasonics,"*IEEETransactions*, vol. 25, no. 1, pp.1–6, 1978.
[7] S.W. Flax, G.H. Glover, and N.J. Pelc,"Textural variations in b-mode ultrasonography: a stochastic model," *Ultrasonic Imaging,*vol. 3, no. 3, pp.235–257, 1981.
[8] G. Kossoff, WJ Garrett, DA Carpenter, J. Jellins,and MJ Dadd,, "Principles and classification of soft tissues by grey scale echography," *Ultrasound in Medicine & Biology*, vol. 2, no. 2, pp. 89–105, 1976.
[9] F.G Sommer, L.F Joynt, BA Carroll, and A. Macovski, "Ultrasonic characterization of abdominal tissues via digital analysis of backscattered waveforms,"*Radiology,*vol. 141, no. 3, pp. 811–817, 1981.
[10] L.F. Joynt, "A stochastic approach to ultrasonic tissue characterization,"PhD thesis, Stanford University, Carlifornia, USA, 1979.
[11] T. Eltoft. "The rician inverse Gaussian distribution: a new model for non-rayleigh signal amplitude statistics."*Image Processing,IEEE Transactions on,* vol..14, no. 11, pp. 1722– 1735, 2005.
[12] O.Francois. "Global optimization with exploration/selection algorithms and simulated annealing,"*The Annals of Applied Probability*, vol. 12,no. 1, pp. 248–271, 2002.
[13] E. Brusseau, C.L. de Korte, F. Mastik, J. Schaar, and A.F.W. van derSteen, "Fully automated luminal contour segmentation in intracoronary ultrasound imaging-a statistical approach," *Medical Imaging, IEEE Transactionson,*vol. 23, no. 5, pp. 554–566, 2004.
[14] M. Mignotte, J. Meunier, and J.C. Tardif, "Endocardial boundary estimation and tracking in echocardiographic images using deformable template and markov random fields,"*Pattern Analysis & Applications,*vol. 4, no. 4, pp. 256–271, 2001.
[15] J. Richy, "Compressive Sensing in Medical Ultrasonography". PhD thesis, KTH, 2012.
[16] M. Kohli, Youtube.(2012, June 20), "Ultrasound Physics 2 – Interactions with tissue", [Video File], http://www.youtube.com/watch?v=Q1YPZ-04dag
[17] T.F. Cootes and C.J. Taylor, "Active shape models - smart snakes," in *Proc. British Machine Vision Conference*,vol. 266275, Citeseer, 1992.
[18] T.F. Cootes, C.J. Taylor, D.H. Cooper, J. Graham, et al, "Active shape models-their training and application," *Computer vision and image understanding,*vol. 61, no. 1, pp. 38– 59, 1995.
[19] T. Cootes.,"An introduction to active shape models," Image Processing and Analysis, pp. 223–248, 2000.
[20] M.B. Stegmann and D.D. Gomez, "A brief introduction to statistical shape analysis,"*Informatics and Mathematical Modelling*, Technical University of Denmark, DTU, pp.15, 2002.
[21] K.W. Wan, K.M. Lam, and K.C. Ng, "An accurate active shape model for facial feature extraction,"*Pattern Recognition Letters*, vol. 26, no. 15, pp. 2409–2423, 2005.
[22] F. Destrempes, J. Meunier, M.F. Giroux, G. Soulez, and G. Cloutier, "Segmentation in ultrasonic¡ emphasis," *MedicalImaging, IEEE Transactions on*, vol. 28, no. 2, pp. 215–229, 2009
[23] B.S. Garra D.G. Brown M.F. Insana, R.F. Wagner and T.H. Shawker, "Analysis of ultrasound image texture via generalized ricianstatistics,"*Optical Engineerin*g, vol. 25, no. 6, pp. 743–748,1986.
[24] P.M.Shankar. "A compound scattering pdf for the ultrasonic echo envelope and its relationship to k and nakagami distribution,"*IEEETransactions,Ferroelect., Freq. Contol*
[25] P.M. Shankar,"A general statistical model for ultrasonic scattering from tissues,"*IEEE Trans. Ultrasonic.Ferroelect., Freq. Contol*
[26] Y.Meiry, YouTube, (2012, Jan 13), "Lecture 13 (Basics of MRI, Ultrasound,", [Video File] http://www.youtube.com/watch?v=w3Ybm4A2GhI
[27] D.Kroon, University of Twente, Febuary2010., [Code]
[28] R. Werner, Allianz, Group Risk Controlling, (2006, May 1) [Code], Germany
[29] J. L. Romeu, "The Chi-Square: a large Sample Goodness of Fit Test," *Reliability Analysis Center,* vol. 10, no. 4, pp. 1-6, START 2003-2004.